Proceedings of the 2018 IEEE
International Conference on Robotics and Biomimetics
December 12-15, 2018, Kuala Lumpur, Malaysia

Autonomous Aerial Manipulation Using a Hexacopter Equipped with a Robotic Arm

Ran Jiao[1], Mingjie Dong[2], Wusheng Chou[13], Hailong Yu[1] and Hao Yu[1]

***Abstract*— This paper presents the implementation of an autonomous aerial manipulation using a hexacopter equipped with a two DOF robotic arm. The kinematic and dynamic models are developed by considering the dynamic characteristics of the combined manipulation platform. A novel adaptive sliding mode controller is proposed for both position and velocity control. By building SSD (Single Shot Detection) deep neural network based on deep learning, an object detection solution is developed. The three dimensional coordinates of the target object relative to the multirotor are obtained via combining the vertical plane position obtained from object detection law with the depth value from stereo camera. Finally, with the proposed controller and object detection law, an autonomous flight experiment is accomplished including approaching, grabbing and delivering the target object. The proposed approaches are demonstrated with effectiveness and could be utilized in various manipulation applications.**

I. INTRODUCTION

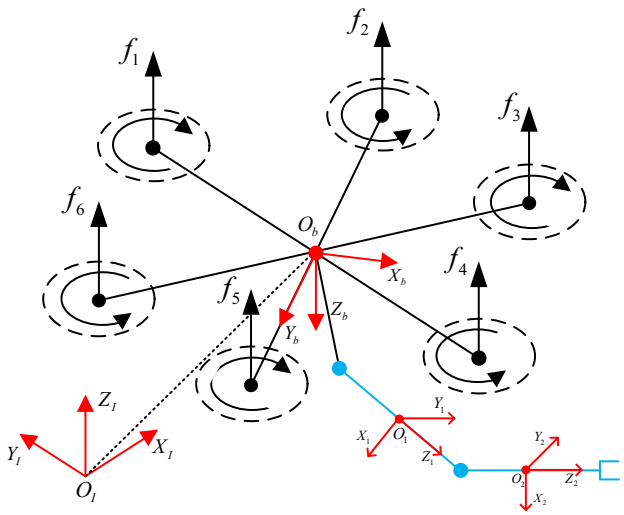

Fig. 1. Hexacopter and robotic arm system with coordinate reference frames

Unmanned Aerial Vehicles (UAVs), which are increasingly used as human assistants in various aspects in recent years, would be utilized on new application scenarios requiring not only the autonomous flight but also interaction with outer environment. Based on that, much interest is given to utilize them for aerial manipulation which could access regions not easily envisaged by land or water. To this end, a robotic arm is equipped on the UAV as shown in Fig. 1.

The capability to execute aerial manipulation requires suitable mechanical structure. A light compliant arm is designed and verified in experiment for aerial manipulation in [1]. Moreover, work [2] proposes appropriately designed grippers for aerial grasping processes. Additionally, there are also many experiments on aerial manipulation. In [3], an aerial transportation task is conducted in which a wood block is grabbed and released by a quadrotor, while in [4], an object is transported by two cooperation quadrotors. Moreover, a relatively large object is picked up by several quadrotors cooperatively in [5]. In [6], a UAV is utilized for the manipulation of an object on a prescribed trajectory. The applications of UAV are not limited to transportation. A large, sustained force is applied on the environment by the quadrotor in [7]. Similarly, a task of docking maneuver is performed by the aerial manipulator in [8].

Nevertheless, the dynamics equation of the multirotor is highly coupled with the motion of the robotic arm. Additionally, the reaction forces from interacting with the object or outer environment would also be an important reason for decreasing the stability of the UAV.

To overcome that issue, plenty of control methods have been proposed recently. Work [9] proposes an impedance control scheme for aerial robotic manipulators. Moreover, a passivity-based adaptive controller based on sliding mode is presented in [10] for both position and velocity control. Based on the dynamics model, a backstepping controller is proposed in [11].

Additionally, automatic flight of UAV is much more popular and beneficial in our life. It will be really better if the aerial manipulator is able to be guided by visual information and transports a target object autonomously. An omnidirectional camera and an eye-in-hand camera are used for offering visual guidance information based on image-based visual servo (IBVS) method, which could be found in [10] and [12], respectively. However, the visual conducting method mentioned above has disadvantages, which is lack of intelligence and could not detect objects in various species.

To deal with that issue, the method of object detection based on deep learning has been proposed in recent years. However, deep learning is not the latest technology. Its first utilization could be dated back to 1971 when Ivakhnenko trained an 8-layer neural network[13]. The important reason for the popularization of deep learning method is the fast de-

[1]College of Mechanical Engineering and Automation, Beihang University, Beijing, P.R. China
[2]College of Mechanical Engineering and Applied Electronics Technology, Beijing University of Technology, Beijing, P.R. China.
[3]The State Key Laboratory of Virtual Reality Technology and Systems, Beihang University, Beijing, P.R. China
Corresponding author:Wusheng Chou Email: wschou@buaa.edu.cn

978-1-7281-0376-1/18/$31.00 ©

velopment of CUDA(Compute Unified Device Architecture) for Nvidia GPUs. On the basis of that, so many methods are proposed for detecting objects using deep neural networks, such as Faster R-CNN(Region-based Convolutional Neural Network)[14], You Only Look Once(YOLO)[15], SSD[16], etc. Numerous tests have been conducted for the approaches mentioned above(SSD 59 FPS with mAP(Mean Average Precision) 74.3% , Faster R-CNN 7 FPS with mAP 73.2% and YOLO 45 FPS with mAP 63.4% on VOC2007 test). SSD and Faster R-CNN are obviously more appropriate after the intercomparison of accuracy. However, the required computation of Faster R-CNN is too large to load on embedded systems because of the demand of instantaneity. The utilization of deep neural networks is as follows. A novel approach based on deep neural network used as a supervised image classifier is proposed to perceive forest or mountain trails from a single monocular image in [17]. Similarly in [18], the DeepFly is presented for autonomous navigation of a quadcopter equipped with monocular camera. The deep neural network is used to predict bounding boxes for multiple navigable regions whose input is the disparity map from performing a translation maneuver. Additionally, a machine learning approach is conducted for target detection when UAV replicates highly adaptive avian perching behavior[19]. Moreover, work[20] presents a deep learning for UAVs Landing carrier in different conditions.

In this work, a hexacopter aerial vehicle equipped with a manipulation system is studied. A unified dynamics model of hexacopter-manipulator system is proposed in the controller design. In additional, an adaptive controller based on sliding mode is presented for the whole system. Then an object detection method based on SSD is used and loaded on NVIDIA Jetson TX2. Finally, an experiment of autonomous aerial manipulation is implemented.

The outline of this paper is structured as follows. In section II, the kinematic and dynamic models of the hexacopter-manipulator system are provided. The adaptive controller is presented in section III. In section IV, by building SSD, the object detection method is developed. The experiments of target object detection and autonomous aerial manipulation are presented in section V. Finally, section VI concludes the paper.

II. KINEMATIC AND DYNAMIC MODEL

The kinematic and dynamic models of the hexacopter combined with a two DOF manipulator as unified forms are presented in this section. More details about deriving kinematic and dynamic models could be obtained in [21].

A. Kinematic Model

As shown in Fig. 1, several coordinates are defined as follows.

O_I: the world-fixed inertial reference frame.

O_{b}: the body-fixed reference frame with origin at the center of geometry in hexacopter.

O_i: the coordinate system fixed to the robotic arm i. The subscript $(i = 1, 2)$ represents the link number.

The absolute position of O_{b} with respect to O_I is denoted by $p^I = [x, y, z]^T$. Meanwhile, the attitude angle is described by Euler angles $\xi = [\phi, \theta, \psi]^T$. Let $\eta = [\eta_1, \eta_2]^T$ represents the joint angles of the robotic arm relative to the zero position. The vector containing all the generalized variables is given by $q = [(p^I)^T, \xi^T, \eta^T]^T \in R^{8\times1}$. Moreover, let $\dot{p}^I$ describe the absolute linear velocity of the aerial vehicle, while $\dot{p}^b$ denotes the linear velocity of the aerial vehicle with respect to O_{b}. The absolute rotational velocity of the aerial vehicle is given by $\omega^{\mathrm{I}}=[\omega_x^I, \omega_y^I, \omega_z^I]^T$. Meanwhile, $\omega^b = [\omega_x^b, \omega_y^b, \omega_z^b]^T$ denotes the rotational velocity of the UAV with respect to O_{b}. Then the following equations could be obtained.

$$\dot{p}^I = R_B \dot{p}^{\mathrm{b}} \tag{1}$$

$$\omega^{\mathrm{I}} = R_T \dot{\xi} \tag{2}$$

$$\omega^b = (R_B)^T \omega^I = (R_B)^T R_T \dot{\xi} = R_Q \dot{\xi} \tag{3}$$

Where $R_T \in R^{3\times3}$ denotes the transformation matrix which converts Euler angle rates $\dot{\xi}$ into ω^{I}. $R_B \in R^{3\times3}$ is the rotation matrix denoting the orientation of O_{b} with respect to O_I, and $R_Q=(R_B)^T R_T \in R^{3\times3}$ maps the time derivative of ξ into the UAV angular velocity expressed in O_{b}.

The position of the frame O_i, attached to the manipulator, with respect to O_I, is given by

$$p_i^I = p^I + R_B p_i^b \tag{4}$$

Where the vector p_i^b represents the position of O_i with respect to O_{b}, expressed in O_{b}. Moreover, the following relationship are considered

$$\dot{p}_i^b = J_{pi} \dot{\eta} \tag{5}$$

$$\omega_i^b = J_{ri} \dot{\eta} \tag{6}$$

Where the ω_i^b denotes the angular velocity of the i-th manipulator frame with respect to O_{b}. The Jacobian matrix $J_{pi} \in R^{2\times2}$ and $J_{ri} \in R^{2\times2}$ relate the translational and angular velocities of each manipulator link to the $\dot{\eta}$, respectively. Deriving (4) with respect to time and considering (5) and (6), the translational and angular velocity of O_i respect to O_I could be given by

$$\dot{p}_i^I = \dot{p} + S(\omega^I) R_B p_i^b + R_B J_{pi} \dot{\eta} \tag{7}$$

$$\omega_i = \omega^I + R_B J_{ri} \dot{\eta} \tag{8}$$

Where $S(\cdot)$ denotes the skew-symmetric matrix.

B. Dynamic Model

The dynamic model of the hexacopter plus robotic arm system could be derived by using the Euler-Lagrange formulation. More details are available in [21]. The system dynamics can be given by

$$M(q)\ddot{q} + C(q, \dot{q})\dot{q} + G(q) = T + T_{ext} \tag{9}$$

Where $M(q) \in R^{8\times8}$ is the symmetric positive definite inertia matrix. $G(q) \in R^{8\times1}$ is the vector of gravitational

terms. The (8×1) vector T and T_{ext} represent the generalized input forces and external disturbance applied to the system, respectively. The last $C(q,\dot{q})$ is the matrix of Coriolis and centrifugal terms whose generic element is given by

$$c_{ij}=\sum_{k=1}^{8}\frac{1}{2}(\frac{\partial m_{ij}}{\partial q_k}+\frac{\partial m_{ik}}{\partial q_j}-\frac{\partial m_{kj}}{\partial q_i})\dot{q}_k \tag{10}$$

Where m_{ij} represents the the generic element of $M(q)$ at the ith row and jth column.

As shown in Fig. 1, by supposing negligible the aerodynamic effects, the vector T has the following expression

$$T=\bar{R}_B N f=\Xi f \tag{11}$$

Where $f=[f_v^T,\bar{\eta}^T]^T$, f_v and $\bar{\eta}$ represent the (6×1) input vector of forces given by the hexacopter motors and the (2×1) input vector of the manipulator joint torques, respectively. In addition, $\bar{R}_B$, as a (8×8) matrix, could be given by $\bar{R}_B=diag(R_B,{R_Q}^T,I_2)$. And $N=diag(\Psi,I_2)$,in which

$$\Psi=\begin{bmatrix} 0 & 0 & 0 & 0 & 0 & 0\\ 0 & 0 & 0 & 0 & 0 & 0\\ 1 & 1 & 1 & 1 & 1 & 1\\ \frac{d}{2} & d & \frac{d}{2} & -\frac{d}{2} & -d & -\frac{d}{2}\\ -\frac{\sqrt{3}d}{2} & 0 & \frac{\sqrt{3}d}{2} & \frac{\sqrt{3}d}{2} & 0 & -\frac{\sqrt{3}d}{2}\\ c_d & -c_d & c_d & -c_d & c_d & -c_d \end{bmatrix} \tag{12}$$

Where d is the distance from a motor to the center of the hexacopter and c_d denotes the drag factor.

III. ADAPTIVE CONTROLLER

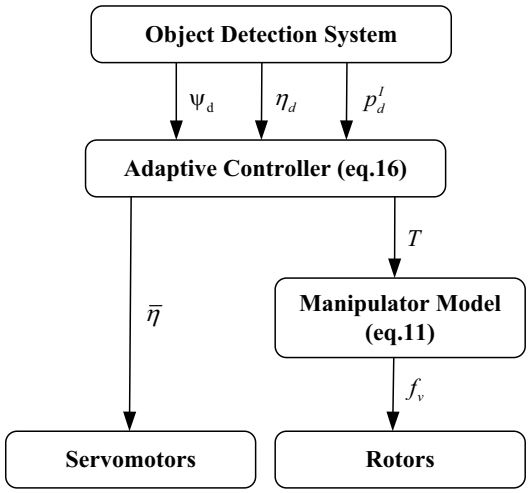

Fig. 2. Control scheme of the aerial manipulation system.

The full dynamic model of a hexacopter with a robotic arm is a complex mathematical structure owing to the dynamical couplings existing between the vehicle and the manipulator. In this section, an adaptive controller based on sliding mode for the combined system presented in section II is built. To realize aerial manipulation, the UAV will be faced with several challenges. First, the extension or retrieval of the robotic arm will disturb the entire system, so will the pick or release of an object during the aerial operation. The stability of the UAV should be ensured under the controller. In addition, accurate position control is of great importance during aerial manipulation, but it would be easily influenced by the motion of robotic arm or the external force and torque. In brief, the robustness and adaptivity of the controller are the key issues for aerial manipulation.

The designed adaptive controller is composed of two systems. System one is a traditional controller similar to the one in [3], which would easily give rise to the oscillation of the actual status values around the desired ones. Therefore system one is only responsible for part of both the position control of the vehicle and the joint angles control of the robotic arm. When the desired values are transmitted from external commander, the period before the first overlap of the actual and desired values is under the control of system one and the rest is controlled by system two. Moreover, system two is also responsible for the whole attitude control. Compared to the controller in [10], an integral term is added in the whole proposed control system to achieve better robustness and eliminate steady state errors. The design of the control system with integral action for UAV was early provided in [22].

At the beginning of the controller design, the sliding surface s and error e are given by

$$e=q-q_d \tag{13}$$

$$\dot{q}_r=\dot{q}_d-\Lambda e-\int e d\tau \tag{14}$$

$$s=\dot{q}-\dot{q}_r=\dot{e}+\Lambda e+\int e d\tau \tag{15}$$

Where $\Lambda\in R^{8\times8}$ is a diagonal matrix with positive elements. Based on the combined model (9), the control law could be derived by

$$T=\hat{M}\ddot{q}_r+\hat{C}\dot{q}_r+\hat{G}-K_c e+\hat{\Delta} \tag{16}$$

Where $\hat{M}$, $\hat{C}$ and $\hat{G}$ represent the estimation of the original matrix. $\hat{\Delta}$ describes the estimated uncertainty. In addition, $K_p\in R^{8\times8}$ is a positive gain matrix. Combining (9), we could derive:

$$\hat{M}\dot{s}+\hat{C}s+K_c e=\tilde{\Delta} \tag{17}$$

Where

$$\tilde{\Delta}=\hat{\Delta}-\Delta \tag{18}$$

$$\Delta=-\tilde{M}\ddot{q}-\tilde{C}\dot{q}-\tilde{G}-T_{ext} \tag{19}$$

$$\tilde{M}=\hat{M}-M \tag{20}$$

$$\tilde{C}=\hat{C}-C \tag{21}$$

$$\tilde{G}=\hat{G}-G \tag{22}$$

In the equations above, $\sim$ represents the error between the estimation and original one.

Then the complementary sliding mode surface is chosen to build the Lyapunov function. The generalized sliding mode

surface and the complementary sliding mode surface are given by

$$S_{e1} = e + K_e \int e d\tau \tag{23}$$

$$S_{e2} = e - K_e \int e d\tau \tag{24}$$

Where K_e is a positive gain matrix. We consider the Lyapunov function :

$$V = \frac{1}{2}\{s^T \hat{M} s + \tilde{\Delta}^T \Gamma \tilde{\Delta} + S_{e1}^T \Gamma_e S_{e1} + S_{e2}^T \Gamma_e S_{e2}\} > 0 \tag{25}$$

Where Γ, Γ_e are positive gain matrixes.

Then we define:

$$\dot{\hat{\Delta}} = -\Gamma^{-1} s \tag{26}$$

With the skew symmetricity of $\dot{\hat{M}} - 2\hat{C}$, the derivative of V with respect to time could be derived according to (15):

$$\begin{aligned} \dot{V} &= s^T \hat{M} \dot{s} + \tfrac{1}{2} s^T \dot{\hat{M}} s + \tilde{\Delta}^T \Gamma \dot{\tilde{\Delta}} + S_{e1}^T \Gamma_e \dot{S}_{e1} + S_{e2}^T \Gamma_e \dot{S}_{e2} \\ &= s^T(-K_p e + \tilde{\Delta}) + \tilde{\Delta}^T \Gamma \dot{\tilde{\Delta}} + 2 e^T \Gamma_e (\dot{e} + {K_e}^2 \textstyle\int e d\tau) \\ &= -\Lambda e^T K_p e + \tilde{\Delta}^T (\Gamma \dot{\tilde{\Delta}} + s) \end{aligned} \tag{27}$$

Where $K_c = 2\Gamma_e$ is requested. In addition, K_e is needed to be an identity matrix. we adopt that $\dot{\Delta} \approx 0$, namely the Δ changes very slow. Then it will be satisfied that

$$\dot{V} = -\Lambda e^T K_p e \leq 0 \tag{28}$$

From the theory of Lyapunov stability, we could get $S_{e1} \to 0$, $S_{e2} \to 0$, $s \to 0$, $\tilde{\Delta} \to 0$. These mean that $e \to 0$, $\dot{e} \to 0$, $\int e d\tau \to 0$ are satisfied. In that condition, the whole system tends to be stable.

On the basis of the designed adaptive controller, the whole control scheme of the aerial manipulation system could be obtained in Fig. 2. The target positions of both aerial vehicle and robotic arm are generated from 'Object Detection System' block which is the top layer in the control scheme. Based on (16), the target positions are transported to 'Adaptive Controller' block from which the control parameters would then be acquired. Included in the parameter T, the target lift force and torques are transmitted to the 'Manipulator Model' block. According to (11), the torques of all the propellers f_v could be ultimately obtained, respectively.

IV. OBJECT DETECTION SYSTEM

In order to realize successful autonomous aerial manipulation, the vehicle is required to have the ability to perceive where the target is. In recent years, deep learning techniques for object detection have been implemented on numerous applications. The SSD[16] is more accurate and much faster than the methods that utilize an additional object proposal step, and it is built and utilized for object detection in this section. In addition, the SSD is based on a feed-forward convolutional network and it could produce several fixed-size bounding boxes in which object class instances would be scored.

Moreover, SSD is an extension and integration network based on the Faster RCNN and YOLO. Predictions from multiple feature maps are combined with different resolutions in SSD for detecting objects in different sizes. Additionally, removing bounding box proposals and the succeeding pixel or feature resampling phases give rise to the improvement in speed for object detection. The overall objective loss function is given by

$$L(x, c, l, g) = \frac{1}{N}(L_{conf}(x, c) + \alpha L_{loc}(x, l, g)) \tag{29}$$

where the meanings of parameters mentioned above could be found in [16].

V. EXPERIMENT

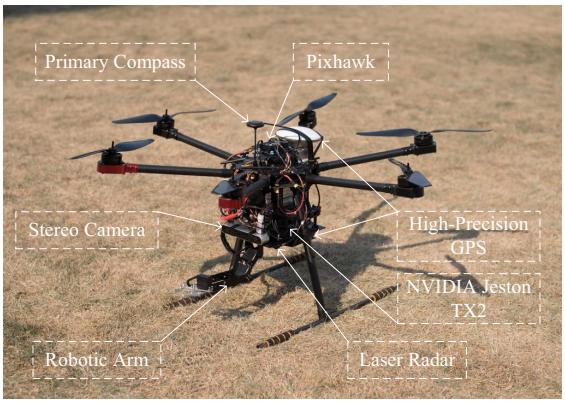

Fig. 3. Prototype of the proposed aerial manipulator.

In this section, all the previous theories presented in Section III and IV, are validated by implementing a series of experiments. As shown in Fig. 3, the flight vehicle is a hexacopter with a 143cm tip-to-tip wingspan, 17-inches propellers, height of 58cm and a total mass of 10.5kg including the two DOF robotic arm. Several assistant sensors and equipments are assembled on the vehicle. The robotic arm driven by servomotors with high torque is equipped under the hexacopter. With 6 CPU cores and 256 CUDA cores, NVIDIA Jetson TX2 is used as the platform for target object detection and computation of control information. Combined with object detection law, the stereo camera above robotic arm is utilized for obtaining three dimensional coordinates of the target object relative to the vehicle. The primary compass is fastened on the highest place to escape from electromagnetic interference. A laser radar is fixed under the vehicle to measure the height of the vehicle relative to the ground with its frequency 100Hz. The high-precision GPS placed on the vehicle is used to provide accurate information of relative and absolute position of the hexacopter. The open source pixhawk fixed on the top is mainly responsible for sensor collection, attitude computation, mode switch, state inspection, security regime, etc.

A. Object Detection Experiment

In this subsection, as shown in Fig. 4, an experiment of target detection is conducted on the playground. The

(a) (b)

Fig. 4. Results of target detections using SSD loaded on NVIDIA Jeston TX2. (**a**) Tripod detection. (**b**) Medicine bottle detection.

input image is a screenshot of the video transcribed from stereo camera. The SSD network could create scores for the presence of each object category and generate adjustments to the box to match the shape of object better.

The total 2956 training frames with a size of 600×600 are used in our experiment as training dataset. These frames were collected in several different environments. The dataset has been divided into disjoint training set (2365 frames) and testing set (591 frames). To avoid that the same trail section appears in both the training and testing set, the split was defined carefully. The detection model is trained on a computer equipped with a NVIDIA TITAN XP, achieving 75.6% mAP and then the model is loaded on the NVIDIA Jeston TX2. We fine-tune the resulting model using mini-batch gradient descent with batch size 24, initial learning rate 0.002, 0.9 momentum optimizer value and 0.0004 weight decay. It is verified that the detection system has a frame rate of 5 FPS on NVIDIA Jeston TX2.

B. Grasping Experiment

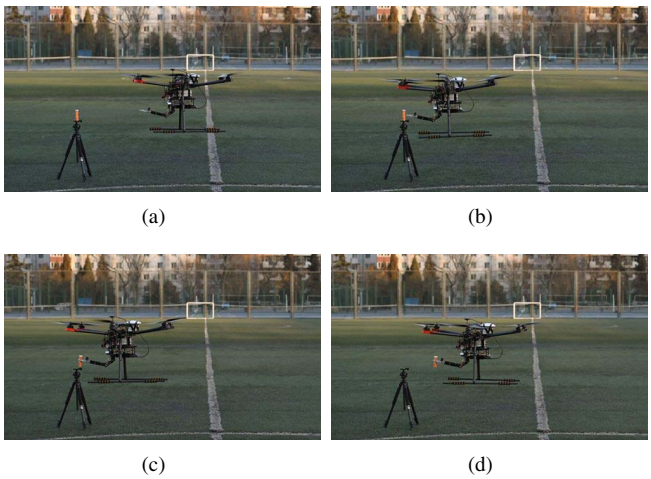

(a) (b)

(c) (d)

Fig. 5. The process of Grasping experiment on the playground. (**a**)The hexacopter is approaching the target. (**b**)The hexacopter is about to grab the target medicine bottle. (**c**)The medicine bottle is picked up. (**d**)The hexacopter moves back to home.

In this subsection, an auto gripping task experiment is performed on the playground as shown in Fig. 5. The grasping target is a medicine bottle shown in Fig. 4(b).

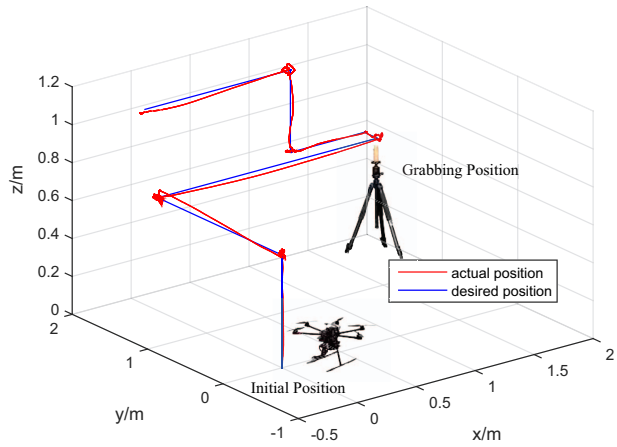

Fig. 6. The desired and actual trajectory of the end effector through the experiment.

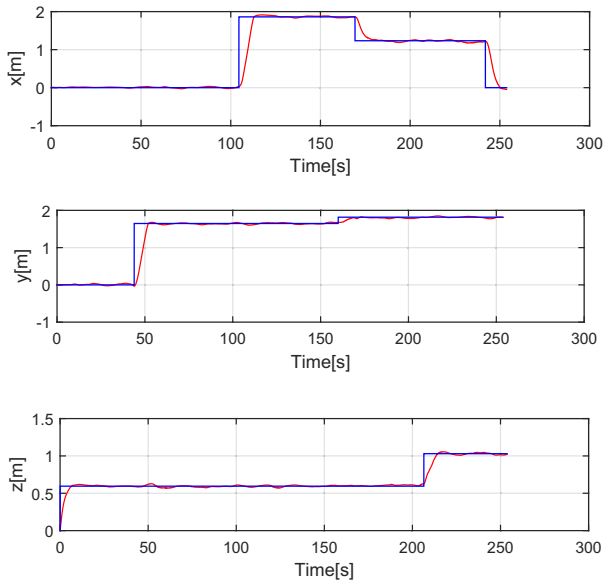

Fig. 7. The respective desired and actual position of the end effector through the experiment.

When the vehicle is about to take off, the target object is located far from it, so the image of the medicine bottle is too small to detect. However, it is relatively easy to detect the tripod whose three dimensional location could be obtained by combining the object detection law with stereo camera. Then the accurate location of the medicine bottle relative to vehicle would be acquired as the vehicle approaches it. According to (4), the position of the end effector in vehicle could be obtained. Then the whole desired and actual moving trajectories of the end effector are described in Fig. 6. Moreover, the desired and actual positions of x,y and z axes are shown in Fig. 7, respectively. To verify the robustness of the proposed controller, an experiment of stretching the robotic arm during the flight of vehicle is conducted. The desired and actual θ during the stretch of the robotic arm is

shown in Fig. 8. Besides, the difference between actual and desired θ is given in Fig. 9. At the beginning, the actual θ could follow the variational rules of desired θ with difference less than 1 degree. The robotic arm stretches at the time marked with light blue dotted line. This motion has been immediately detected by the adaptive controller designed in section III. After about 0.4 seconds, the difference between the actual and desired θ goes back to the status similar to the beginning.

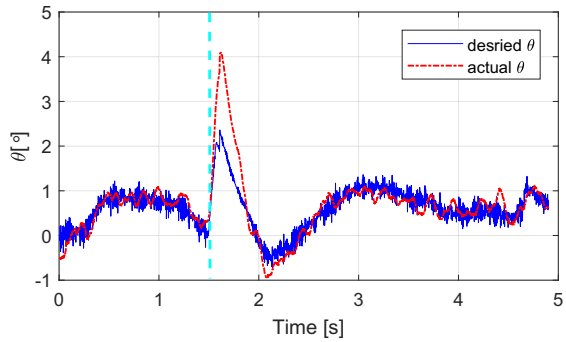

Fig. 8. The desired and actual θ during the stretch of the robotic arm. The start time of stretching robotic arm is marked with light blue dotted line.

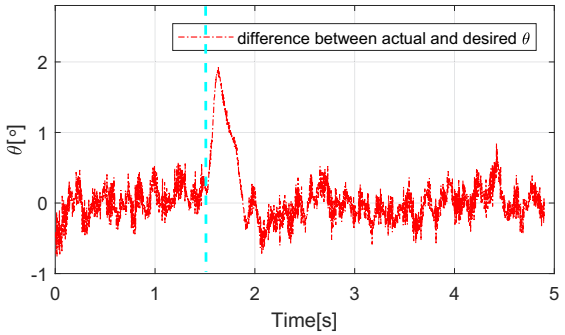

Fig. 9. Difference between actual and desired θ during the stretch of the robotic arm. The start time of stretching robotic arm is marked with light blue dotted line.

VI. CONCLUSIONS

In this paper, an autonomous aerial manipulation system is presented. The kinematic and dynamic models as a combined form for the multirotor aerial vehicle equipped with a two DOF robotic arm are presented. Moreover, a novel adaptive controller based on sliding mode has been proposed for the aerial manipulation system. An object detection system based on SSD is loaded on NVIDIA Jetson TX2. Finally, an experiment of autonomous aerial manipulation to grasp a medicine bottle is conducted, which demonstrates satisfactory implementation to execute the given tasks.

ACKNOWLEDGMENT

This work was supported by the National Natural Science Foundation of China under Grant 61633002.

REFERENCES

[1] Suarez, Alejandro, G. Heredia, and A. Ollero. "Lightweight compliant arm for aerial manipulation." Ieee/rsj International Conference on Intelligent Robots and Systems IEEE, 2015, pp. 1627-1632.
[2] Mellinger, Daniel, et al. "Design, modeling, estimation and control for aerial grasping and manipulation." Intelligent Robots and Systems (IROS), 2011 IEEE/RSJ International Conference on. IEEE, 2011, pp. 2668-2673.
[3] Kim, Suseong, Seungwon Choi, and H. Jin Kim. "Aerial manipulation using a quadrotor with a two dof robotic arm." Intelligent Robots and Systems (IROS), 2013 IEEE/RSJ International Conference on. IEEE, 2013, pp. 4990-4995.
[4] Caccavale, Fabrizio, et al. "Cooperative impedance control for multiple UAVs with a robotic arm." Intelligent Robots and Systems (IROS), 2015 IEEE/RSJ International Conference on. IEEE, 2015, pp. 2366-2371.
[5] Mellinger, Daniel, et al. "Cooperative grasping and transport using multiple quadrotors." Distributed autonomous robotic systems. Springer, Berlin, Heidelberg, 2013, pp. 545-558.
[6] Srikanth, Manohar, et al. "Controlled manipulation with multiple quadrotors." AIAA Guidance, Navigation, and Control Conference. 2011, p. 6547.
[7] Wopereis, H. W., et al. "Application of substantial and sustained force to vertical surfaces using a quadrotor." Robotics and Automation (ICRA), 2017 IEEE International Conference on. IEEE, 2017, pp. 2704-2709.
[8] Forte, Francesco, et al. "On the control of an aerial manipulator interacting with the environment." Robotics and Automation (ICRA), 2014 IEEE International Conference on. IEEE, 2014, pp. 4487-4492.
[9] Cataldi, Elisabetta, et al. "Impedance Control of an aerial-manipulator: preliminary results." Intelligent Robots and Systems (IROS), 2016 IEEE/RSJ International Conference on. IEEE, 2016, pp. 3848-3853.
[10] Kim, Suseong, et al. "Vision-guided aerial manipulation using a multirotor with a robotic arm." IEEE/ASME Transactions On Mechatronics 21.4 (2016), pp. 1912-1923.
[11] Jimenez-Cano, A. E., et al. "Control of an aerial robot with multilink arm for assembly tasks." Robotics and Automation (ICRA), 2013 IEEE International Conference on. IEEE, 2013, pp. 4916-4921.
[12] Liu, Ming, Cedric Pradalier, and Roland Siegwart. "Visual homing from scale with an uncalibrated omnidirectional camera." IEEE Transactions on Robotics 29.6 (2013), pp. 1353-1365.
[13] Ivakhnenko, Alexey Grigorevich. "Polynomial theory of complex systems." IEEE transactions on Systems, Man, and Cybernetics 4 (1971), pp. 364-378.
[14] Ren, Shaoqing, et al. "Faster r-cnn: Towards real-time object detection with region proposal networks." Advances in neural information processing systems. 2015, pp. 91-99.
[15] Redmon, Joseph, et al. "You only look once: Unified, real-time object detection." Proceedings of the IEEE conference on computer vision and pattern recognition. 2016, pp. 779-788.
[16] Liu, Wei, et al. "Ssd: Single shot multibox detector." European conference on computer vision. Springer, Cham, 2016, pp. 21-37.
[17] Giusti, Alessandro, et al. "A machine learning approach to visual perception of forest trails for mobile robots." IEEE Robotics and Automation Letters 1.2 (2016), pp. 661-667.
[18] Shah, Utsav, R. Khawad, and K. M. Krishna. "DeepFly: towards complete autonomous navigation of MAVs with monocular camera." the Tenth Indian Conference 2016, pp. 1-8.
[19] Luo, Cai, L. Yu, and P. Ren. "A Vision-aided Approach to Perching a Bio-inspired Unmanned Aerial Vehicle." IEEE Transactions on Industrial Electronics PP.99(2017), pp. 1-1.
[20] Zhou, Dinale, et al. "Deep learning for unmanned aerial vehicles landing carrier in different conditions." Advanced Robotics (ICAR), 2017 18th International Conference on. IEEE, 2017, pp. 469-475.
[21] Lippiello, Vincenzo, and Fabio Ruggiero. "Cartesian impedance control of a UAV with a robotic arm." IFAC Proceedings Volumes 45.22 (2012), pp. 704-709.
[22] Bouabdallah, S., Siegwart, R. Y. (2007). Full control of a quadrotor. In IEEE/RSJ International Conference on Intelligent Robots and Systems, 2007: IROS 2007; Oct. 29, 2007-Nov. 2, 2007, pp. 153-158.